Water Resources Research

Key Points:
- A theoretical framework is presented that introduces a dimensionless number for computing the evaporation from unsaturated soils
- Evaporation can be limited by either air or the soil side of the land surface depending on the value of dimensionless number
- Laboratory experiments in an uncontrolled environment were used to validate the theoretical framework

Supporting Information:
- Supporting Information S1

Correspondence to:
A. de la Fuente,
aldelafu@ing.uchile.cl

Evaporation From Unsaturated Soils as a Function of the Air and Soil Sides of the Land Surface

Pedro de Amesti[1], Alberto de la Fuente[1] , and Francisco Suárez[2,3,4]

[1]Departamento de Ingeniería Civil, Universidad de Chile, Santiago, Chile, [2]Departamento de Ingeniería Hidráulica y Ambiental, Pontificia Universidad Católica de Chile, Santiago, Chile, [3]Centro de Desarrollo Urbano Sustentable (CEDEUS), CONICYT/FONDAP/15110020, Santiago, Chile, [4]Centro de Excelencia en Geotermia de los Andes (CEGA), CONICYT/FONDAP/15090013, Santiago, Chile

Abstract A theoretical framework for computing the evaporation from unsaturated soils is presented and validated based on laboratory experiments that were conducted in an uncontrolled environment where forcing variables vary in time according to diurnal meteorological cycles. This theory introduces a dimensionless number that controls the ratio between the actual and potential evaporation from unsaturated soils. The dimensionless number depends on the transfer velocity, which characterizes evaporation into the atmosphere, the diffusion coefficient of water vapor in the soil, and the water table depth. We show that depending on the value of the dimensionless number, evaporation can be limited by either the air-side or the soil-side of the land surface. For large transfer velocity values, evaporation is controlled by water vapor diffusion in the soil, while for shallow water tables, evaporation is controlled by water vapor transport from the land surface into the atmosphere. Despite the good agreement between the shape of the observed and predicted evaporation rates, a fitted dimensionless parameter is required to match the predicted evaporation rates. Possible explanations for this disagreement are given in the discussion.

Plain Language Summary This article seeks to understand and quantify the hydrological cycle in closed basins that are found in the Altiplano region of the Andes Cordillera of South America. These closed basins are found in the desert and, by definition, have no outflow rivers, so the water that precipitates in the catchment must be completely evaporated within the catchment. An important part of this evaporation occurs in the open wetlands (many of which are protected by both national and international laws), which are found in the central depression of the basin, as well as in from the surrounding desert, where groundwater is located at a certain depth below the land surface. In this article, we propose and validate a simple expression for computing soil water evaporation and conduct laboratory experiments in an uncontrolled environment where air and soil temperatures, air humidity, and wind speed vary over time according to diurnal meteorological cycles.

1. Introduction

Evaporation into the atmosphere is a process that can be understood as part of either the surface energy budget or a water vapor transport toward the atmosphere (Brutsaert, 1982; Stull, 1988). From the water vapor transport point of view, the air humidity is usually less than 100% in the atmosphere, whereas near wet surfaces, the concentration of water vapor is saturated. Consequently, a vertical gradient of water vapor concentration is produced, which drives a diffusive mass flux of water vapor from the surface into the atmosphere (Adams et al., 1990; Brutsaert, 1982). In this way, evaporation can be written as follows:

$$E = -k_t \left(\rho_{v\infty} - \rho_{vi} \right) \tag{1}$$

where E denotes evaporation expressed as ($kg_{H_2O}/m^2/s$), k_t is the transfer velocity (m/s), $\rho_{v\infty}$ is the water vapor concentration (kg_{H_2O}/m^3) far away from the surface, and ρ_{vi} is the water vapor concentration (kg_{H_2O}/m^3) at the surface. Note that kg_{H_2O} and kg_{air} are used to differentiate between water vapor mass and air mass, respectively. Both $\rho_{v\infty}$ and ρ_{vi} can be written as follows (Brutsaert, 1982; Stull, 1988):

$$\rho_v = \rho_a q = 0.622 \rho_a \frac{e_a}{P - e_a} \approx 0.622 \rho_a \frac{e_a}{P} \tag{2}$$

where ρ_a denotes the air density (kg_{air}/m^3), q (kg_{H_2O}/kg_{air}) is the mixing ratio, e_a is the partial pressure of water vapor (Pa), and P is the air pressure (Pa). k_t is a flow-dependent parameter (Adams et al., 1990; Garratt, 1992) whose value in field conditions can be obtained by considering the Prandtl mixing length theory that leads to the logarithmic vertical profiles of both the air velocity and water vapor concentration (Adams et al., 1990; Garratt, 1992), which provides the following:

$$k_t = \frac{\kappa^2}{\ln^2\left(\frac{z}{z_o}\right)} u(z) \tag{3}$$

where $u(z)$ is the wind speed measured at an elevation z, z_o is the hydrodynamic surface roughness, and $\kappa = 0.41$ is the von Karmann constant. Corrections to these logarithmic profiles can be considered depending on the atmospheric boundary layer stability (Adams et al., 1990; Garratt, 1992; Mahrt et al., 1984). Finally, it is important to note that if Equation 3 is used, then ρ_{vi} is the water vapor concentration at the hydrodynamic surface roughness z_o, which is detailed as follows.

In saturated surfaces such as lakes or the ocean, the water vapor concentration at the surface ρ_{vi} is known and computed to be the saturated water vapor concentration ($\rho_{v_{sat}}$) that depends on the surface temperature (Brutsaert, 1982; Garratt, 1992). This evaporation is hereinafter called the potential evaporation, which is defined as

$$E_{max} = -k_t\left(\rho_{v\infty} - \rho_{vsat}\right) \tag{4}$$

In unsaturated soils, the value of ρ_{vi} is smaller than the saturated water vapor concentration, such that the actual evaporation from unsaturated soils is a smaller value than the evaporation from wetted surfaces E_{max}. In particular, it is necessary to account for all the transport mechanisms that mobilize water vapor from the evaporative surface toward the land surface and the surface roughness, from which the water vapor diffuses toward the atmosphere according to Equation 1. In this context, laboratory and field studies have shown that the water table depth below the surface (d) is a key parameter that determines the evaporation from unsaturated soils (Kampf et al., 2005; Or et al., 2013; Shokri & Or, 2011; Shokri & Salvucci, 2011; Wang, 2015), where the actual evaporation decreases with d (Lehmann et al., 2008; Or et al., 2013). Lehmann et al. (2008) identified two different stages in evaporation as a function of d (see also Or et al., 2013). In stage 1, the land surface is connected to the water table because capillary forces lift liquid water toward the land surface, where it is evaporated (Shokri & Salvucci, 2011). This occurs if $d < \delta$ (Lehmann et al., 2008; Sadeghi et al., 2012; Yiotis et al., 2006), where δ denotes the thickness of the capillary region and the land surface presents moist patches surrounded by dry areas. During stage 1, water vapor diffuses across the diffusive sublayer, while the land surface is not entirely covered by liquid water but is rather composed by several water filled pores surrounded by dry areas. Consequently, radial diffusion of water vapor from water filled pores toward dry areas of the land surface can become a limiting factor ($E/E_{max} < 1$) for water vapor transport across the diffusive sublayer depending on two dimensionless numbers that are formed based on the ratio between the pore size, the spacing between water filled pores, and the thickness of diffusive sublayer length scales (Schlünder, 1988; Shahraeeni et al., 2012).

In contrast, when $d > \delta$, the land surface is dry and the value E/E_{max} decreases with $\xi = d - \delta$. Shokri and Or (2011) showed that the vertical diffusion of water vapor across ξ is the transport mechanism that mobilizes water vapor toward the atmosphere. Sophisticated models that consider vertical transport of water (liquid and gas phases) from the water table to the surface can be implemented for computing E (Hernández-López et al., 2014, 2016; Sakai et al., 2009). However, these models require solving the water transport equations in the soil and coupling them to the atmospheric boundary layer (Davarzani et al., 2014), which makes them difficult to use in hydrological systems where surface water and ground water interact. Examples of these systems include the closed basins that are found in the Altiplano region of the Andes Mountains (Cabrol et al., 2009; de la Fuente & Niño, 2010; Hernández et al., 2016; Risacher et al., 2003), whose hydrological cycle is also closed such that all the precipitation is completely evaporated within the
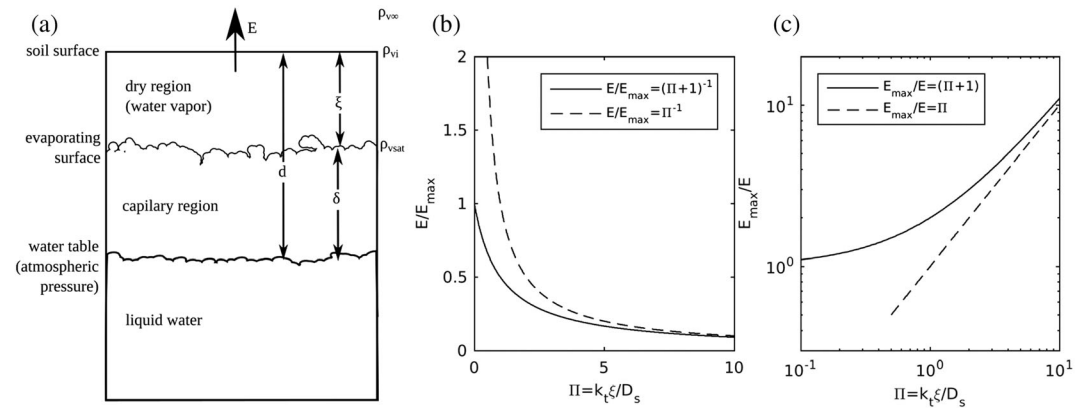
Figure 1. (a) Conceptual scheme for vertical transport of water vapor into the atmosphere. (b) Ratio of E/E_{max} as a function of Π for the solution of Equation 6 (solid line) and Equation 9 (dashed line); (c) similar to (b) for the ratio E_{max}/E.

basin (de la Fuente & Meruane, 2017; de la Fuente & Niño, 2010; Uribe et al., 2015). Attention is placed on wetlands that are found in the central depressions of these basins. These wetlands are formed by groundwater upwelling, whose extension is determined by evaporation from wet and unsaturated soils as well as the terminal saline lakes that are usually found in these systems.

The objective of this article is to present and analyze the results of laboratory-scale experiments that aimed to measure evaporation from unsaturated soils and to relate it to the water table depth and water vapor transport in the atmospheric boundary layer. The novelty of these experiments is that they were conducted in an uncontrolled environment where air and soil temperatures, air humidity, and wind speed vary in time according to diurnal meteorological cycles. These uncontrolled conditions enable to understand the influence of water transport within the soil on evaporation with respect to the water vapor transport in the atmospheric boundary layer and to identify that E/E_{max} is a function of a dimensionless number, $\Pi = k_t \xi / D_s$, where D_s is the water vapor diffusion coefficient modified by soil tortuosity (Moldrup et al., 2000).

2. Methods

2.1. Conceptual Framework

Here, we understand evaporation as a transport process that mobilizes water vapor from the soil into the atmosphere. This transport occurs across the land surface, which is an interface located at $z = 0$ (with z positive upwards), with two faces: the air side ($z = 0^+$) and the soil side ($z = 0^-$) of the land surface. Flux and value continuity are the shared boundary conditions that link both sides of the interface, with ρ_{vi} the unknown water vapor concentration at the land surface and E the vertical flux of water vapor that crosses the land surface. At the air side of the land surface, evaporation is a diffusive flux that is generally written as Equation 1. Below the land surface, the water table is located at a depth d, above which the transport of liquid water through the capillary region of thickness δ also supports evaporation (Figure 1a). Between the capillary region and the land surface, there is a dry region of thickness ξ, across which the water vapor should pass through to explain the evaporation flux at the surface (Lehmann et al., 2008; Shokri et al., 2008). For a constant value of δ, the thickness of the dry region is equal to $\xi = max(0, d - \delta)$ such that ξ is equal to 0 if the water table depth is smaller than δ and evaporation occurs at the land surface. Consequently, we assume that $E/E_{max} = 1$ during stage 1, such that the horizontal diffusion of water vapor at the surface (Schlünder, 1988) and the rate at which capillary effects transport liquid water toward the atmosphere (Shahraeeni et al., 2012) are both large. The validity of this assumption is addressed in section 4. Furthermore, if $d > \delta$, the evaporative plane occurs within the soil, and water vapor crosses the dry region to reach the land surface. Transport processes in this dry region include water vapor diffusion previously identified by Shokri et al. (2008, 2009), so the evaporation can be written as follows:

$$E = -D_s \frac{\partial \rho_v}{\partial z} \qquad (5)$$

where D_s denotes the molecular diffusion coefficient of water vapor in air corrected by sediment tortuosity (Moldrup et al., 2000). Consequently, assuming that E is uniform, the exact solution of (4) is

$$E = -\frac{D_s}{\xi}\left(\rho_{v_i} - \rho_{v_{sat}}\right) \qquad (6)$$

The diffusion coefficient modified by soil tortuosity, D_s, depends on the diffusion coefficient of water vapor in the air ($D = 2.12 \times 10^{-5}(T/(T + 273.15))^2$ m^2/s, where T is the air temperature, in °C, see Hernández-López et al., 2014), the volumetric air content (θ_a), and the sediment porosity (φ), and several expressions can be used to represent it (Moldrup et al., 2000; Scanlon et al., 2002). In this article, we tested the following expressions: $D_s/D = \theta_a^{2.5}/\varphi$, 0.66φ, $\theta_a^{3/2}$, $\theta_a^{4/3}$, $0.435\,\varphi$, and $\theta_a^{7/3}$ (see Table 8.2 of Scanlon et al., 2002). We also assumed that the volumetric air content is constant within the dry region (Figure 1) and equals to the sediment porosity. Note that Equations 5 and 6 are valid only if the evaporation plane is placed inside the soil, not when evaporation occurs at the surface of the soil.

Finally, the expression for computing E is written as follows:

$$E = \frac{1}{1 + \Pi}\,E_{max} \qquad (7)$$

where E_{max} is defined in Equation 4, and

$$\Pi = \frac{k_t \xi}{D_s} \qquad (8)$$

is a dimensionless number that quantifies the influence of water vapor transport in the soil with respect to water vapor transport in the air side of the land surface. Equation 7 is obtained by substituting Equation 6 into Equation 1 to obtain ρ_{v_i}, which is later replaced in either Equation 1 or Equation 6.

Figure 1b plots E/E_{max} as a function of Π, and Figure 1c plots the ratio E_{max}/E as a function of Π. Figures 1b and 1c show that for small values of Π the actual evaporation approaches the potential evaporation, which is thus controlled by the air side of the soil surface, such that $E/E_{max} = 1$ or

$$E = -k_t\left(\rho_{v\infty} - \rho_{v_{sat}}\right) \qquad (9)$$

In contrast, large values of Π are associated with deep water tables or large values of k_t, so the actual evaporation is controlled by water vapor transport in the soil as follows:

$$\frac{E}{E_{max}} = \frac{1}{\Pi} \;\; ; \;\; E = -\frac{D_s}{\xi}\left(\rho_{v\infty} - \rho_{v_{sat}}\right) \qquad (10)$$

Finally, Equation 7 can be written as

$$E = -\frac{k_t}{1 + \Pi}\left(\rho_{v\infty} - \rho_{v_{sat}}\right) = -\frac{D_s}{\xi}\frac{\Pi}{1 + \Pi}\left(\rho_{v\infty} - \rho_{v_{sat}}\right) \qquad (11)$$

Thus, the equivalent transfer velocity $k_e = k_t/(1 + \Pi) = \frac{D_s}{\xi}\Pi/(1 + \Pi)$ can be defined to compute the evaporation from unsaturated soils. Notice that $\rho_{v_{sat}}$ is the saturated water vapor concentration at the evaporative surface and depends on the temperature of the water that is evaporated.

2.2. Experimental Methods and Data Process

The experimental facility was installed on the terrace of the civil engineering building at the Universidad de Chile (supporting information Figure S1). The experimental facility is composed of two circular tanks 300 mm in diameter and 450 mm in height (tanks A and B), which were filled in the same way with

coarse sand with particle diameters between 0.5 and 1 mm. The water table depth is variable in tank A, which was fully saturated at the beginning of the experiments. Tank A was mounted on a balance that was used to measure the evaporation, and it has a piezometer to measure the depth to the water table. Here, we define the water table depth as the depth at which the water pressure equates to the atmospheric pressure. In contrast, tank B was connected to a 150-mm diameter and 430-mm height Mariotte tank, which was used to maintain saturated conditions on the surface of tank B at all times. Both tank B and the Mariotte tank were mounted on balances to measure the evaporation rate of tank B, which indicates the potential evaporation. Continuous measurements of the mass of both tanks and the Mariotte tank were obtained with digital cameras that took images every hour during daylight. The use of blue dye can be used to identify the depth of the evaporative front (Assouline et al., 2014; Shokri et al., 2008).

Further instruments used during the experiments include two HOBO Pendant® Temperature/Light 64 K data logger thermistors to measure the soil temperature in both tanks every 10 min. These temperature measurements are representative of the average temperature in the soil upper layer (~2 cm). Similarly, one soil moisture sensor (Degacon Device GS1) was installed in tank A to record the average moisture in the soil upper layer (~3 cm), which was used to compute the degree of soil saturation. Finally, the air temperature, pressure, and relative humidity near the experimental facility were recorded every 10 min with a standard Campbell meteorological station.

In total, four experiments were conducted at 10.2, 6.4, 3.7, and 2.2 days of duration. Each of these experiments started with tank A filled with water, which evaporated over time.

With respect to the data process, the evaporation for the ith measurement was computed as the slope of the linear fit of the mass per unit of surface area of the tank as a function of time, using the seven measurements neighboring i. Mass observations were conducted every 1 h, and the 95% confidence interval of the slope was used to estimate the error of the observed evaporation. Evaporation under saturated conditions was computed using the total mass of tank B and the Mariotte tank, while the evaporation as a function of d was computed using the mass of tank A. The maximum evaporation of tank A was estimated as $E_{max} = E_B$, where E_B is the evaporation of tank B computed with the slope of the mass as a function of time. Finally, the transfer velocity k_t, which characterizes water vapor diffusion in the air, was determined as $k_t = E_B / \left(\rho_{v\infty} - \rho_{v\,sat}^B \right)$ (see Equation 1), where $\rho_{v\infty}$ is computed with the measured air temperature, air pressure, and relative humidity and $\rho_{v\,sat}^B$ is the saturated water vapor concentration using the soil temperature of tank B. Therefore, we assumed that the water temperature in tank B was the representative value for the water that is evaporated inside the soil of tank A.

2.3. Soil Properties

The soil properties were measured in the hydrogeology laboratory of the Hydraulic and Environmental Engineering Department of Pontificia Universidad Católica de Chile. These properties are as follows:

Soil porosity (n) was measured with a balance, water, and a recipient that is capable of measuring volumes by adding dry soil to the recipient with water and measuring the displaced water to obtain the soil volume. Three different observations were made, obtaining $n = 0.4 \pm 0.006$.

The saturated hydraulic conductivity of the soil (K_W) was measured using a constant-head permeameter (KSAT, METER Group, USA). Nine different measurements were made to characterize the soil, obtaining $K_W = 80 \pm 12.5$ m/day.

The capillarity region thickness, δ (Figure 1), is a key parameter whose actual value is uncertain. To estimate it, we used the soil water retention curve, which was measured in the laboratory with a HYPROP apparatus (METER Group, USA). The laboratory water retention curve was processed by fitting a line in the portion of the retention curve with larger gradients, and the intercept of this line with a saturation degree equal to 1 defines the point where the suction head is equal to the air-entry value, whereas the intercept with a saturation degree equal to 0 defines the evaporation plane. This adopted methodology is similar to the method used by Lehmann et al. (2008), who first fitted the curve of van Genuchten (1980) to the measurements and then used this fitted curve for determining the straight line that is intercepted to the saturation degree equal to 0 and 1. Alternatively, we also estimated δ based on the in situ measurements at the experimental facility for the water table depth and the water content that was measured with the soil moisture
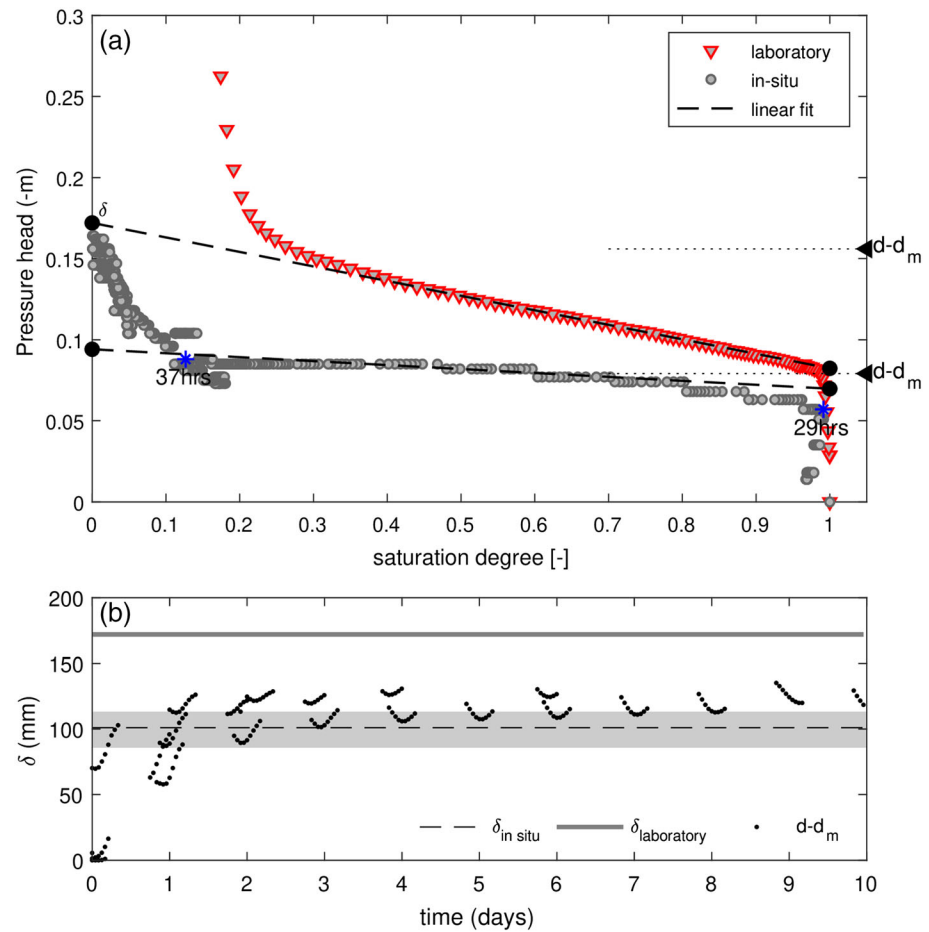
Figure 2. (a) Soil water retention curves and (b) time series of the capillary region thickness estimated based on the water retention curves and the time series of the mass of tank A. The blue star and associated text indicate the number of hour after the experiment started at which this observation occurred.

sensor in tank A. This information allows us for obtaining a pseudo retention curve that was processed in the same way as the laboratory retention curve for estimating δ. Finally, we define the depth d_m, which is computed based on the mass of tank A, as the depth at which the air-water interface would exist if all of the liquid water in the tank were located below it. As a consequence, the capillary region thickness can be estimated as $\delta = d - d_m$, where d_m is computed as follows:

$$d_m(t) = \frac{(M_o - M(t))}{\rho A n} \tag{12}$$

where A denotes the surface area of tank A, n is the soil porosity, ρ is the water density, M_o denotes the initial mass of tank A, and $M(t)$ is the mass of tank A measured with the balance at time t.

3. Results

3.1. Capillary Region Thickness

The general overview of the measurements is shown in supporting information Text S1. As detailed in the soil properties subsection of the methods, the soil water retention curve and the in situ measurements in tank A were computed to characterize the capillary region thickness. Figure 2a shows the laboratory retention curve and the in situ measurements for the 10.2-day-long experiment. The corresponding values of δ were 172 and
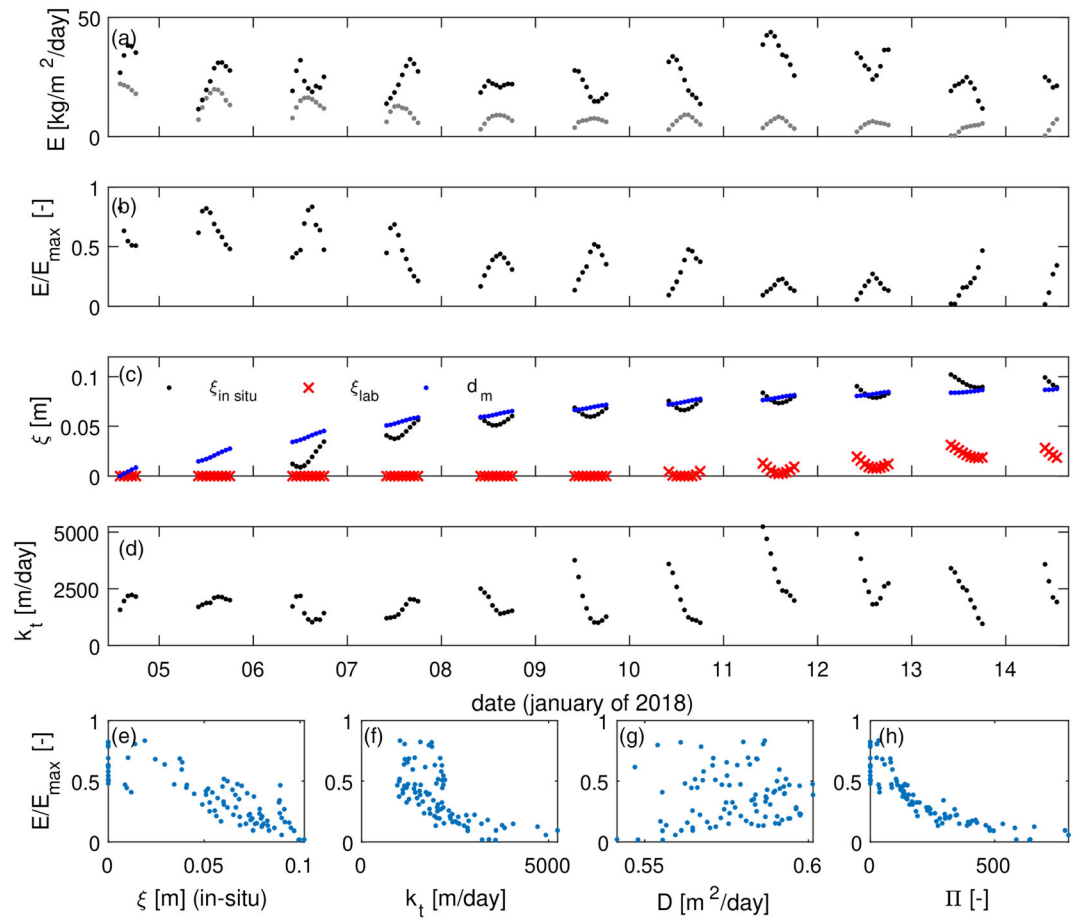
Figure 3. Time series of computed variables: (a) evaporation from tank A and B (gray and black dots, respectively); (b) ratio E/E_{max}; (c) the dry region of thickness ξ estimated with the in situ water retention curve ($\xi_{in\ situ}$), the laboratory retention curve (ξ_{lab}), and the mass of tank A (d_m); and (d) the transfer velocity k_t. (e–g) The ratio E/E_{max} as a function of the different variables involved in Π and (h) the ratio E/E_{max} as a function of Π.

85.6 mm. Furthermore, Figure 2a shows the capillary region thickness estimated as $\delta = d - d_m$, at which all the liquid water would be placed with a saturation degree equal to 1. The curves in Figure 2 show that important differences are obtained when the capillary region thickness is computed based on laboratory retention curve or in situ measurements. In particular, the in situ value of δ was smaller than that measured in the laboratory. The average value of δ obtained for all the in situ measurements was 100.1 $\pm$ 8.3 mm, and this value is used in this article to compute $\xi = d - \delta$. Similarly, the thickness $d - d_m$ computed for the laboratory soil water retention curve was 156 mm, while $d - d_m$ computed for the in situ measurements was 89.9 $\pm$ 10.5 mm. The thickness $d - d_m$ is 90% of δ estimated based on the in situ measurements.

The different estimations of the capillary region thickness δ and $d - d_m$ are shown in Figure 2b, where it is observed that the δ estimated based on the mass of tank A initially grows until reaching a constant value that is larger than that based on the in situ measurements, but smaller than the δ value estimated with the laboratory water retention curve. The impact of the different values of δ on evaporation is given in the following section, while in the discussion we identify possible explanations for the different values of the water retention curves estimated in the laboratory and the in situ curve.

3.2. Dimensionless Number

For the same experiment shown in supporting information Figures S2 and 3 plots the time series of the computed variables that are used for validating the definition of the dimensionless number Π of Equation 7.
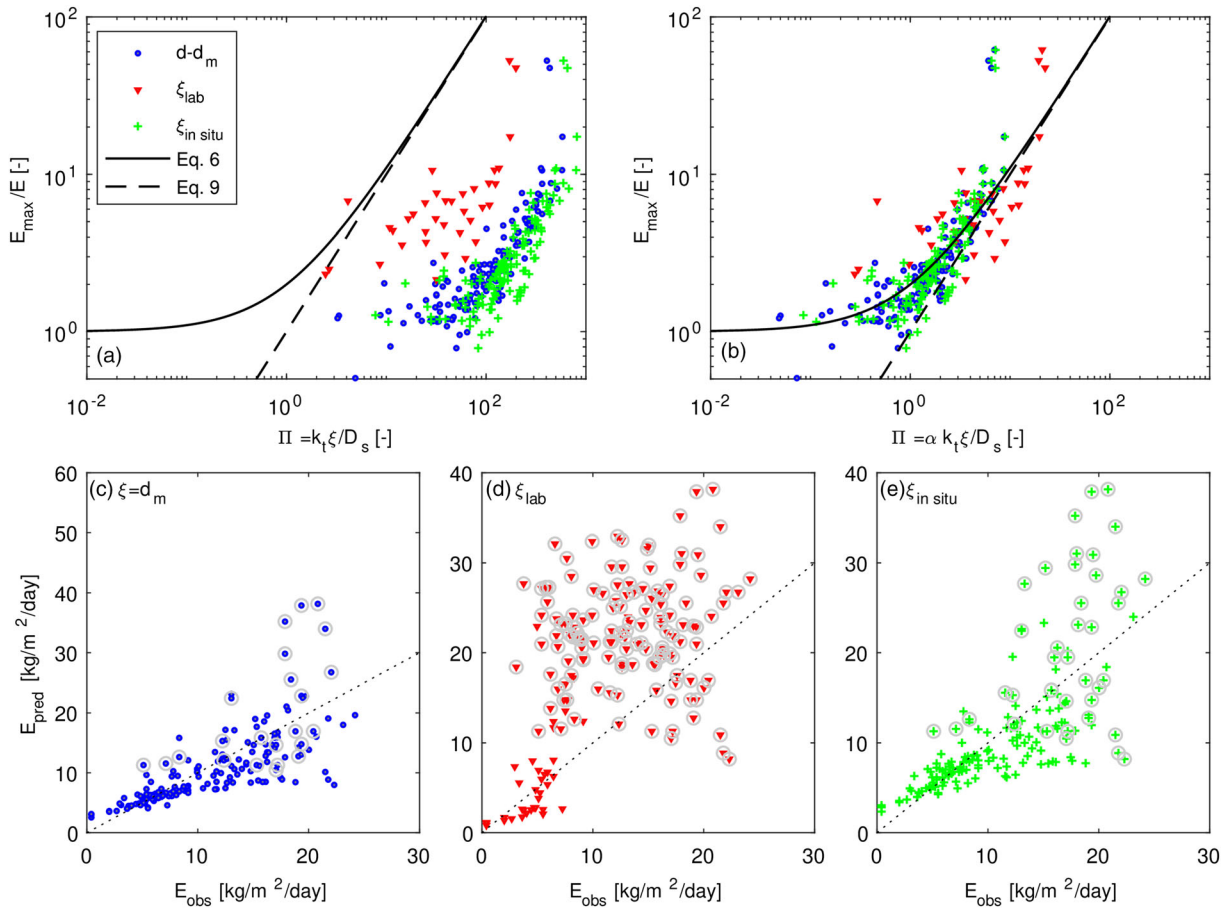
Figure 4. (a) Comparison between E_{max}/E and Π computed with the molecular diffusion coefficient in the soil. (b) Comparison between E_{max}/E and $\alpha\Pi$ with α = 0.0285, 0.2169, and 0.021 for Π computed with $\xi = d_m$, ξ_{lab}, and $\xi_{in\ situ}$, respectively. (c–e). Comparison between the observed and predicted evaporation for $\xi = d_m$, ξ_{lab}, and $\xi_{in\ situ}$. Data with a gray circle indicate evaporation that is associated with $\Pi = 0$ ($\xi = 0$) when the evaporative plane is at the land surface.

Figure 3a shows the time series of evaporation from tanks A and B (gray and black dots, respectively), and Figure 3b plots the ratio E/E_{max}, where E_{max} was computed with Equation 10 and E corresponds to the evaporation from tank A. Evaporation from both tanks varies within the day in response to changes in the environmental conditions (temperature, air humidity, and wind speed). The maximum instantaneous values of evaporation were observed at noon, reaching values as high as 40 $kg_{H_2O}/m^2/day$. As expected, the maximum evaporation was observed in tank B, which always had saturated conditions on the land surface. In contrast, the evaporation from tank A decreased over time in response to the deepening of the water table. The values of E/E_{max} during the first days were larger than 0.9, whereas by the end of the experiment, E/E_{max} had values smaller than 0.2. Finally, Figure 3c plots the time series of ξ for each one of the adopted methodologies, whose value varies between 0 and 10 cm, and Figure 3d plots the time series of the transfer velocity k_t that report values in the range of 500 and 5,000 m/days.

The validation of the use of Π for computing E/E_{max} is shown in Figures 3e–3h, where Figures 3e–3g plot the ratio E/E_{max} as a function of the different variables required for evaluating Π, showing that none of the variables are solely able to explain the changes in the evaporation with respect to the maximum evaporation. However, once we plot E/E_{max} as a function of Π (Figure 3h), it can be seen that all the data collapse into a single curve, which supports the use of this dimensionless number. Furthermore, to evaluate the use of the analytic expression of Equation 5 for quantifying this relationship between E/E_{max} and Π, Figure 4a shows the direct comparison between the measured values of E_{max}/E and Π for all four experiments,

where Π was computed with $\xi_{in\ situ}$, ξ_{lab}, and d_m, and $D_s = D\theta_a^{2.5}/\varphi$ (Moldrup et al., 2000). Figure 4a shows that although the shape of the measurements follows the analytical solution of Equation 5 (black solid line), the measurements are shifted toward the right of the plot with respect to the analytic solution. This observation is particularly true for Π computed with $\xi_{in\ situ}$ and d_m, while the use of Π computed with ξ_{lab} presents a larger dispersion with respect to the analytical solution of Equation 5. The shift toward the right in the plot suggests that the dimensionless number Π can be corrected by a factor α such that the product $\alpha\Pi$ is used in Equation 7, with α being a fitted dimensionless parameter. For $D_s = D\theta_a^{2.5}/\varphi$ (Moldrup et al., 2000), the fitted values of α were $\alpha = 0.0149\% \pm 11\%$, $0.1128\% \pm 30\%$, and $0.011\% \pm 11\%$ for the Π computed with $\xi = d_m$, ξ_{lab}, and $\xi_{in\ situ}$, respectively. Similar results were obtained for the rest of the expressions tested for computing D_s, with fitted values of α between 0.0103 and 0.0174 for $\xi = d_m$, α between 0.078 and 0.1315 for $\xi = \xi_{lab}$, and α between 0.008 and 0.013 for $\xi = \xi_{in\ situ}$. The main results shown in Figure 4b are not sensitive to the specific model for computing D_s.

Finally, Figures 4c–4e compare the measured evaporation from tank A with the predicted evaporation using Equation 7 and $D_s = D\theta_a^{2.5}/\varphi$. The errors in the cumulative evaporation for all the measurements were equal to 4%, 61%, and 1% for $\xi = d_m$ (Figure 4c), ξ_{lab} (Figure 4d), and $\xi_{in\ situ}$ (Figure 4e). The disagreement between the measured and predicted evaporation using the laboratory water retention curve (ξ_{lab}) can be explained by the large value of $\delta = 172$ mm so that the evaporation from tank B is predicted to be equal to the potential evaporation for a wider range of d, thus overestimating the actual evaporation. However, this explanation assumes that k_t computed based on tank A is representative of the conditions in tank B, which may not be true as discussed below.

4. Discussion

4.1. Dimensionless Number

We have presented and validated a theoretical background that links processes that occur at both sides of the land surface for computing the evaporation from unsaturated soils: the transport of water vapor from the land surface into the atmosphere and the molecular transport within the soil. The analysis led to a simple algebraic expression for computing evaporation from unsaturated soils (Equation 7), which depends on the dimensionless number $\Pi = k_t\xi/D_s$ that quantifies the effect of soil transport processes in the soil with respect to transport from the land surface into the atmosphere (Figure 1b). For small values of Π, the evaporation from unsaturated soils approaches the potential evaporation and E can be computed with Equation 8 ($E/E_{max} \rightarrow 1$). This limit occurs not only when the water table is near the surface but also for large D_s (e.g., sands or gravels) and small values of k_t (e.g., during calm wind conditions). In contrast, when $\Pi \gg 1$, $E/E_{max} \approx 1/\Pi$, such that the actual rate of evaporation is controlled by transport within the soil. Under these conditions, the evaporation can be computed with Equation 9 and is associated with large values of ξ (e.g., "deep" water table) or k_t (e.g., during windy conditions) and small values of D_s (e.g., clays).

The analysis that leads to Equation 7 considered steady state conditions, thus restricting the analysis to time-scales larger than a characteristic time scale that is associated with the diffusion process of water vapor in the soil. This characteristic timescale, t^*, can be estimated as the characteristic timescale that diffusion takes to act on length ξ, such that $t^* = \xi^2/D_s$. For the experimental conditions presented in this article, the average and maximum values of t^* were 9 and 25 min, respectively. These time steps are much smaller than those from the measurements (every 1 h). Therefore, temporal changes in the water vapor diffusion in the soil can be represented by a sequence of permanent states, each one described by Equation 7.

Our motivation for developing the simple expression of Equation 7 for computing the evaporation from unsaturated soils is that it simplifies the dynamic link between large-scale meteorological processes and basin-scale groundwater transport in the closed basins of the Altiplano region in the Andes Mountains of South America (Costelloe et al., 2009; de la Fuente & Meruane, 2017; Johnson et al., 2010; Suárez et al., 2020). In particular, groundwater in these closed basins upwells toward the terminal wetlands (oases in the desert) where it is completely evaporated; however, the amount of water that directly evaporates from the shallow aquifer is uncertain, and understanding how these unique ecosystems would behave in response to changes in the precipitation and the evaporation is necessary.

4.2. Fitted Dimensionless Parameter α

In this article, the dimensionless parameter α was needed to fit Equation 7 to the laboratory observations. The need for this adjustment suggests that the actual value of the adopted variables required for computing Π is uncertain. Since $\alpha < 1$, it can be because k_t estimated based on tank A is overestimated. In particular, Or et al. (2013) showed that the horizontal transport of water vapor can be a limiting factor for high evaporation rates and for coarse textured media. This microscopic phenomenon can be interpreted as an additional resistance to the vertical diffusion of water vapor that produces a smaller k_t than what was measured in tank A. This additional resistance was reported for large values of k_t and for stage 1 of evaporation (Or et al., 2013; Shahraeeni et al., 2012). If this is the case, additional resistance to the vertical diffusion of water vapor is needed to explain the observed rates of evaporation. The laboratory retention curve may be representative of our experiments, while the measured k_t in tank A would not fully describe the transport process from the surface toward the atmosphere. To account for this extra resistance, Schlünder (1988) obtained a similar expression to our Equation 7 ($E = E_{max}/(1 + \Phi)$) where the dimensionless parameter, Φ, accounts for the additional resistance to the vertical diffusion associated horizontal transport of water vapor on the soil surface, whose value depends on the relative wetted surface area, among other factors.

However, it is important to note that an enhanced diffusion in soils has been previously reported by several authors since the midtwentieth century (Hernández-López et al., 2014; Philip & De Vries, 1957), and to account for these conditions, an enhanced factor is used, whose value ranges between 3 and 18. However, it is also important to note that Shokri et al. (2009) showed that the enhancement factor may not be needed if the correct dry region thickness, ξ, is used for computing evaporation based on the Fick's law. In the context of this article, the enhanced factor is equal to $1/\alpha$, and it takes different values depending on the used parametrization of D_s and form for computing ξ. In particular, $1/\alpha$ takes values between 30 and 75 for $\xi = d_m$, values between 4 and 10 if ξ_{lab} is used, and values between 41 and 102 if $\xi_{in\ situ}$ is used for computing Π. A first estimation suggests that these range of values of $1/\alpha$ can also be explained by radial vapor diffusion, thus reducing the actual value of k_t, as it was detailed in the previous paragraph.

In conclusion, despite the dimensionless number $\Pi = k_t\xi/D_s$ and the expression of Equation 7 presented in this article being representative of the links between processes that occur on both sides of the land surface, further analysis is needed to elucidate the actual values of the dimensional variables k_t, δ, and D_s, particularly under field conditions (Suárez et al., 2020).

4.3. Water Retention Curves

In this article, we estimated the capillary region thickness based on simultaneous in situ measurements of the water content at the land surface and the depth of the atmospheric pressure isobar (the water table depth). These measurements gave us a pseudo retention curve that is different than the retention curve obtained in the laboratory, thus opening new research questions for understanding these differences and for developing methodologies in situ measurements of this key curve. First, for the in situ measurements consider a Lagrange approach that assumes that the water content at a certain height, ℓ, above the atmospheric pressure isobar does not depend on the depth of the atmospheric pressure isobar and is equal to the water content measured on the land surface when the atmospheric pressure isobar was at a depth ℓ below the land surface. This assumption may not always be true and detailed measurements of the water content at different elevations are needed. Second, the difference between the in situ measurements and the laboratory retention curve, as well as the observed changes in the water table depth observed in Figure S2 in the supporting information that showed that the water table raised during the day, suggests that there is a dynamic link between the piezometric head (water retention curve) and evaporation. Shokri and Salvucci (2011) and Sadeghi et al. (2012) noted that the groundwater evaporation must be supported by a vertical flow of liquid water within the capillary region that is described by Darcy's law, $E = -K_W(\theta)\partial h/\partial z$, where h is the pressure head and $K_W(\theta)$ is the unsaturated hydraulic conductivity that depends on the water content (θ). Since K_W does not depend on E, changes in the evaporation rate modify the vertical gradient of h that is steeper for large values of E. Therefore, as the evaporation in the experimental facility is larger than the evaporation in the laboratory apparatus used for measuring the laboratory retention curve, the differences between both retention curves may be explained by the evaporation itself. This dynamic link between the retention curve and evaporation also helps to explain the observed changes in the water table depth observed in Figure S2 of

the supporting information, which showed that the water table was raised during the day. In particularly, the observations in Figure S2 may be due to thermal volumetric expansion/contraction associated with changes in the soil temperature; however, this can also be explained by temporal changes in the piezometric head (water retention curve) in response to changes in evaporation. Finally, it is important to note that the differences between in situ measurements and the laboratory retention curve can be due to the disturbance of the soil produced when collecting the sample that is analyzed in the laboratory. If this is the case, developing an in situ methodology for measuring the water retention curve may contribute to reducing this experimental error.

In future works, the dynamic link between evaporation and the retention curve should be studied in detail, as well as the advantages and disadvantages of using in situ simultaneous measurements of the soil humidity at the land surface and the depth of the atmospheric isobar (the water table depth) for estimating the capillary region thickness.

5. Summary

In this article we showed that the effect of water vapor diffusion within the soil on water evaporation from unsaturated soils can be quantified by the dimensionless number $\Pi = k_t \xi / D_s$. The results are sensitive to the depth of the evaporative plane ξ, the thickness of the capillary region, and the effective water vapor diffusion coefficient within the soil.

Data Availability Statement

Experimental data archiving is available online (https://doi.org/10.34691/FK2/SSBIIT).

References

Adams, E. E., Cosler, D. J., & Helfrich, K. R. (1990). Evaporation from heated water bodies: Predicting combined forced plus free convection. *Water Resources Research*, *26*(3), 425–435. https://doi.org/10.1029/WR026i003p00425

Assouline, S., Narkis, K., Gherabli, R., Lefort, P., & Prat, M. (2014). Analysis of the impact of surface layer properties on evaporation from porous systems using column experiments and modified definition of characteristic length. *Water Resources Research*, *50*, 3933–3955. https://doi.org/10.1002/2013WR014489

Brutsaert, W. (1982). *Evaporation into the atmosphere*. Dordrecht: Springer Science & Business Media. https://doi.org/10.1007/978-94-017-1497-6

Cabrol, N. A., Grin, E. A., Chong, G., Minkley, E., Hock, A. N., Yu, Y., et al. (2009). The High-Lakes Project. *Journal of Geophysical Research*, *114*, G00D06, https://doi.org/10.1029/2008JG000818

Costelloe, J. F., Irvine, E. C., Western, A. W., & Herczeg, A. L. (2009). Groundwater recharge and discharge dynamics in an arid-zone ephemeral lake system, Australia. *Limnology and Oceanography*, *54*(1), 86–100. https://doi.org/10.4319/lo.2009.54.1.0086

Davarzani, H., Smits, K., Tolene, R. M., & Illangasekare, T. (2014). Study of the effect of wind speed on evaporation from soil through integrated modeling of the atmospheric boundary layer and shallow subsurface. *Water Resources Research*, *50*, 661–680. https://doi.org/10.1002/2013WR013952

de la Fuente, A., & Meruane, C. (2017). Spectral model for long-term computation of thermodynamics and potential evaporation in shallow wetlands. *Water Resources Research*, *53*, 7696–7715. https://doi.org/10.1002/2017WR020515

de la Fuente, A., & Niño, Y. (2010). Temporal and spatial features of the thermohydrodynamics of shallow salty lagoons in northern Chile. *Limnology and Oceanography*, *55*(1), 279–288. https://doi.org/10.4319/lo.2010.55.1.0279

Garratt, J. R. (1992). In C. U. Press (Ed.), *The atmospheric boundary layer*. Cambridge: Cambridge University Press.

Hernández, K. L., Yannicelli, B., Olsen, L. M., Dorador, C., Menschel, E. J., Molina, V., et al. (2016). Microbial activity response to solar radiation across contrasting environmental conditions in Salar de Huasco, northern Chilean Altiplano. *Frontiers in Microbiology*, *7*, 1857. https://doi.org/10.3389/fmicb.2016.01857

Hernández-López, M. F., Braud, I., Gironás, J., Suárez, F., & Muñoz, J. F. (2016). Modelling evaporation processes in soils from the Huasco salt flat basin, Chile. *Hydrological Processes*, *30*(25), 4704–4719. https://doi.org/10.1002/hyp.10987

Hernández-López, M. F., Gironás, J., Braud, I., Suárez, F., & Muñoz, J. F. (2014). Assessment of evaporation and water fluxes in a column of dry saline soil subject to different water table levels. *Hydrological Processes*, *28*(10), 3655–3669. https://doi.org/10.1002/hyp.9912

Johnson, E., Yáñez, J., Ortiz, C., & Muñoz, J. (2010). Evaporation from shallow groundwater in closed basins in the Chilean *Altiplano*. *Hydrological Sciences Journal*, *55*(4), 624–635. https://doi.org/10.1080/02626661003780458

Kampf, S., Tyler, S., Ortiz, C., Muñoz, J., & Adkins, P. (2005). Evaporation and land surface energy budget at the Salar de Atacama, northern Chile. *Journal of Hydrology*, *310*(1–4), 236–252. https://doi.org/10.1016/j.jhydrol.2005.01.005

Lehmann, P., Assouline, S., & Or, D. (2008). Characteristic lengths affecting evaporative drying of porous media. *Physical Review E*, *77*(5), 056309. https://doi.org/10.1103/PhysRevE.77.056309

Mahrt, L., Ek, M., Mahrt, L., & Ek, M. (1984). The influence of atmospheric stability on potential evaporation. *Journal of Climate and Applied Meteorology*, *23*(2), 222–234. https://doi.org/10.1175/1520-0450(1984)023<0222:tioaso>2.0.co;2

Moldrup, P., Olesen, T., Gamst, J., Schjønning, P., Yamaguchi, T., & Rolston, D. E. (2000). Predicting the gas diffusion coefficient in repacked soil. *Soil Science Society of America Journal*, *64*(5), 1588–1594. https://doi.org/10.2136/sssaj2000.6451588x

Or, D., Lehmann, P., Shahraeeni, E., & Shokri, N. (2013). Advances in soil evaporation physics—A review. *Vadose Zone Journal*, *12*(4), vzj2012.0163. https://doi.org/10.2136/vzj2012.0163

Philip, J. R., & De Vries, D. A. (1957). Moisture movement in porous materials under temperature gradients. *Eos, Transactions of the American Geophysical Union*, *38*(2), 222. https://doi.org/10.1029/TR038i002p00222

Risacher, F., Alonso, H., & Salazar, C. (2003). The origin of brines and salts in Chilean salars: A hydrochemical review. *Earth Science Reviews*, *63*(3–4), 249–293. https://doi.org/10.1016/S0012-8252(03)00037-0

Sadeghi, M., Shokri, N., & Jones, S. B. (2012). A novel analytical solution to steady-state evaporation from porous media. *Water Resources Research*, *48*, W09516. https://doi.org/10.1029/2012WR012060

Sakai, M., Toride, N., & Šimůnek, J. (2009). Water and vapor movement with condensation and evaporation in a sandy column. *Soil Science Society of America Journal*, *73*(3), 707–717. https://doi.org/10.2136/sssaj2008.0094

Scanlon, B. R., Nicot, J. P., & Massmann, J. W. (2002). Soil gas movement in unsaturated systems. In *Soil physics companion* (pp. 297–341). Boca Raton, FL: CRC Press. https://doi.org/10.1201/9781420041651.ch8

Schlünder, E. U. (1988). On the mechanism of the constant drying rate period and its relevance to diffusion controlled catalytic gas phase reactions. *Chemical Engineering Science*, *43*(10), 2685–2688. https://doi.org/10.1016/0009-2509(88)80012-5

Shahraeeni, E., Lehmann, P., & Or, D. (2012). Coupling of evaporative fluxes from drying porous surfaces with air boundary layer: Characteristics of evaporation from discrete pores. *Water Resources Research*, *48*, W09525. https://doi.org/10.1029/2012WR011857

Shokri, N., Lehmann, P., & Or, D. (2008). Effects of hydrophobic layers on evaporation from porous media. *Geophysical Research Letters*, *35*, L19407. https://doi.org/10.1029/2008GL035230

Shokri, N., Lehmann, P., & Or, D. (2009). Critical evaluation of enhancement factors for vapor transport through unsaturated porous media. *Water Resources Research*, *45*, W10433. https://doi.org/10.1029/2009WR007769

Shokri, N., & Or, D. (2011). What determines drying rates at the onset of diffusion controlled stage-2 evaporation from porous media? *Water Resources Research*, *47*, W09513. https://doi.org/10.1029/2010WR010284

Shokri, N., & Salvucci, G. D. (2011). Evaporation from porous media in the presence of a water table. *Vadose Zone Journal*, *10*(4), 1309–1318. https://doi.org/10.2136/vzj2011.0027

Stull, R. B. (1988). *An introduction to boundary layer meteorology* (Vol. 13). Dordrecht, Boston, London: Kluwer Academic Publishers.

Suárez, F., Lobos, F., de la Fuente, A., de Arellano, J. V. G., Prieto, A., Meruane, C., & Hargensis, O. (2020). E-DATA: A comprehensive field campaign to investigate evaporation enhanced by advection in the hyper-arid altiplano. *Water (Switzerland)*, *12*(3). https://doi.org/10.3390/w12030745

Uribe, J., Muñoz, J. F., Gironás, J., Oyarzún, R., Aguirre, E., & Aravena, R. (2015). Assessing groundwater recharge in an Andean closed basin using isotopic characterization and a rainfall-runoff model: Salar del Huasco basin, Chile. *Hydrogeology Journal*, *23*(7), 1535–1551. https://doi.org/10.1007/s10040-015-1300-z

van Genuchten, M. T. (1980). A closed-form equation for predicting the hydraulic conductivity of unsaturated soils. *Soil Science Society of America Journal*, *44*(5), 892–898. https://doi.org/10.2136/sssaj1980.03615995004400050002x

Wang, X. (2015). Vapor flow resistance of dry soil layer to soil water evaporation in arid environment: An overview. *Water*, *7*(12), 4552–4574. https://doi.org/10.3390/w7084552

Yiotis, A. G., Tsimpanogiannis, I. N., Stubos, A. K., & Yortsos, Y. C. (2006). Pore-network study of the characteristic periods in the drying of porous materials. *Journal of Colloid and Interface Science*, *297*(2), 738–748. https://doi.org/10.1016/J.JCIS.2005.11.043